# Distinguishing Anisotropy and Flexibility of the Pentasaccharide LNF-1 in Solution by Carbon-13 NMR Relaxation and Hydrodynamic Modeling

**Torgny Rundlöf,[†] Richard M. Venable,[‡] Richard W. Pastor,[‡] Jozef Kowalewski,[§] and Göran Widmalm*,[†]**

*Contribution from the Department of Organic Chemistry, Division of Physical Chemistry, Arrhenius Laboratory, Stockholm University, S-106 91 Stockholm, Sweden, and Biophysics Laboratory, Center for Biologics Evaluation and Research, Food and Drug Administration, Bethesda, Maryland 20892*

*Received July 28, 1999. Revised Manuscript Received September 24, 1999*

**Abstract:** Carbon-13 spin−lattice ($T_1$) and spin−spin ($T_2$) relaxation times and $^1H-^{13}C$ NOEs have been measured at four magnetic field strengths (7.0, 9.4, 11.7, and 14.1 T) for a 30 °C $D_2O$ solution of lacto-*N*-fucopentaose-1, a pentasaccharide from human milk. There are significant differences between the residues, with the largest $T_1$, $T_2$, and NOE values for carbons with axial C−H bonds of the 4-substituted glucose unit (**E**) at the reducing end. The data were fit using model free formalism, first with overall rotation assumed to be isotropic and then with rotational anisotropy taken into account. Somewhat improved fits were obtained with the latter, which yielded an anisotropy $D_{||}/D_{\perp} = 1.35-1.5$. The generalized order parameters, $S^2$, for ring carbons of residues **A**−**D** were similar in the two models, and approximately equal to 0.7, though significant differences in both order parameters and internal relaxation times were obtained for residue **E**. As supported by Langevin dynamics simulations, the experimentally derived $S^2$ for the ring carbons of residue **E**, 0.68 for C1 (α-anomeric configuration) and 0.43 for C2 and C3, are best explained by large fluctuations within the minimum of a single dominant conformation. The translational diffusion coefficient, $D_t$, obtained from NMR measurements equaled $1.8 \times 10^{-6}$ cm$^2$ s$^{-1}$. Hydrodynamic calculations on the energy minimized dominant conformation yielded $D_{||}/D_{\perp} = 1.8$ and $D_t = 2.0 \times 10^{-6}$ cm$^2$ s$^{-1}$, assuming one bound water per hydroxyl group and rigid geometry. The difference between the anisotropy fitted from relaxation data and that calculated by hydrodynamics is proposed to be associated with the substantial flexibility at the reducing end.

## Introduction

Oligosaccharides serve as recognition molecules in numerous biological processes.[1] One important class, the antigens in the ABO blood group system, consists of oligosaccharides on glycoproteins and glycolipids with the common backbone structures β-D-Gal*p*-(1→3)-β-D-Glc*p*NAc (type 1) or β-D-Gal*p*-(1→4)-β-D-Glc*p*NAc (type 2). Further glycosylations convert them into specific blood group antigens.[2] Some blood group or blood group related oligosaccharides also show potency as differentiation or tumor-associated antigens.[3]

Knowledge of the conformational flexibility of the carbohydrate moiety is essential for understanding carbohydrate-mediated recognition mechanisms. For example, a conformational entropy loss is anticipated upon binding to a protein,[4] though the importance of this effect has been disputed.[5] Detailed structural information of oligosaccharides in the solid state can be obtained by X-ray crystallography. Unfortunately, oligosaccharides are difficult to crystallize, and little is learned of the dynamics. NMR spectroscopy, often in combination with different molecular modeling techniques,[6,7,8,9] has become a widely used approach for studying the structure and dynamics of oligosaccharides in solution, including blood group oligosaccharides.[10,11] Measurements of $^1H-^1H$ or $^1H-^{13}C$ dipolar couplings in a liquid crystalline medium yield additional structural information.[12,13]

The dynamics are reflected in the spectral density functions determining the carbon-13 $T_1$ and $T_2$ relaxation times and $^1H-^{13}C$ NOE factors.[14] By measuring these parameters for different carbons at a number of magnetic field strengths one obtains detailed information of the overall and internal reorientation.[15,16] There are various methods for interpreting heteronuclear relaxation data in terms of molecular motional parameters. The model-free approach[17] by Lipari and Szabo describes the dynamics of an isotropically tumbling molecule in terms of

[†] Department of Organic Chemistry, Stockholm University.
[‡] Center for Biologics Evaluation and Research, Food and Drug Administration.
[§] Division of Physical Chemistry, Stockholm University.

(1) Dwek, R. A. *Chem. Rev.* **1996**, *96*, 683−720.
(2) Watkins, W. M. *Science* **1966**, *152*, 172−181.
(3) Feizi, T. *Nature* **1985**, *314*, 53−57.
(4) Carver, J. P. *Pure Appl. Chem.* **1993**, *65*, 763−770.
(5) Bundle, D. R.; Alibés, R.; Nilar, S.; Otter, A.; Warwas, M.; Zhang, P. *J. Am. Chem. Soc.* **1998**, *120*, 5317−5318.
(6) Woods, R. J. *Curr. Opin. Struct. Biol.* **1995**, *5*, 591−598.
(7) Woods, R. J. *Glycoconjugate J.* **1998**, *15*, 209−216.
(8) Peters, T.; Pinto, B. M. *Curr. Opin. Struct. Biol.* **1996**, *6*, 710−720.
(9) Rundlöf, T.; Kjellberg, A.; Damberg, C.; Nishida, T.; Widmalm, G. *Magn. Reson. Chem.* **1998**, *36*, 838−847.
(10) Cagas, P.; Kaluarachchi, K.; Bush, C. A. *J. Am. Chem. Soc.* **1991**, *113*, 6815−6822.
(11) Imberty, A. *Curr. Opin. Struct. Biol.* **1997**, *7*, 617−623.
(12) Tjandra, N.; Bax, A. *Science* **1997**, *278*, 1111−1114.
(13) Rundlöf, T.; Landersjö, C.; Lycknert, K.; Maliniak, A.; Widmalm, G. *Magn. Reson. Chem.* **1998**, *36*, 773−776.
(14) Palmer, A. G. *Curr. Opin. Struct. Biol.* **1997**, *7*, 732−737.
(15) Kowalewski, J. *Ann. Rep. NMR Spectr.* **1990**, *22*, 307−414.
(16) Kowalewski, J. *Ann. Rep. NMR Spectr.* **1991**, *23*, 289−374.

10.1021/ja992675b CCC: $18.00 
Published on Web 11/30/1999

overall and internal correlation times and a generalized order parameter related to the spatial restriction of the internal reorientation. It has been applied to studies of proteins and protein/ligand binding,[18,19] nucleic acids,[20,21] and carbohydrates.[22−27] It has been extended to include two distinct correlation times to describe the internal motions,[28] enabling the detection of slower internal motions in proteins. A different approach is the spectral density mapping,[29,30] which uses the full or reduced spectral densities taken at different frequencies to determine overall and internal motions.

Anisotropic overall tumbling of biomolecules in solution has been investigated for proteins[31,32,33] and oligo- and polysaccharides.[34−37] Typically the expressions for a symmetric top model[38] are used to describe the reorientation,[39] though fully anisotropic treatments have also been reported.[32,40]

This report considers the dynamics and flexibility of the pentasaccharide lacto-*N*-fucopentaose-1, α-L-Fuc*p*-(1→2)-*β*-D-Gal*p*-(1→3)-*β*-D-Glc*p*NAc-(1→3)-*β*-D-Gal*p*-(1→4)-D-Glc*p*. Consisting of five residues and extracted from human milk, LNF-1 contains an H-type-1 blood group antigen trisaccharide at the nonreducing end and a glucose residue at the reducing end (a mixture of slowly interconverting α and *β* isomers).[41,42] On the NMR time scale, the α and *β* isomers can be treated as two different compounds[43] with structural differences near the reducing end, resulting in different $^{13}C$ chemical shifts for C1−C3 of the glucose residue of the two isomers. The other carbon resonances analyzed were not resolved; their relaxation behavior is considered an average of the two isomers.

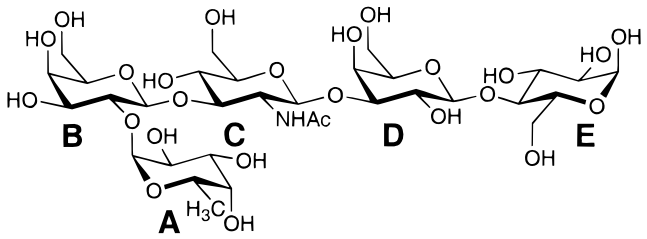


**Figure 1.** Schematic of the pentasaccharide LNF-1 in its α-anomeric configuration. Sugar residues are denoted as **A** (L-fucose), **B** (D-galactose), **C** (*N*-acetyl-D-glucosamine), **D** (D-galactose), and **E** (D-glucose).

Figure 1 shows the molecule in its α-configuration. The molecule is clearly not spherical, and it is therefore reasonable to question whether its tumbling can adequately be described with an isotropic model. If it is not, applying such a model might lead to unphysical parameters, and, consequently, incorrect inferences regarding quantities of interest, such as the flexibility. To more confidently characterize LNF-1, we have measured carbon-13 NMR $T_1$, $T_2$ values and NOE factors in $D_2O$ at 303 K and four different magnetic field strengths and fitted the relaxation parameters using both the isotropic and symmetric top model-free approaches. Additionally, the translational diffusion coefficient for the pentasaccharide was obtained using NMR spin−echo techniques. Hydrodynamic calculations were carried out as an independent check on the derived parameters and to investigate the influence of hydration on translational diffusion and rotational diffusion anisotropy.

## Theory

Relaxation of proton-bearing carbon-13 nuclei is usually dominated by dipole−dipole (DD) interactions with neighboring protons. Assuming that chemical shift anisotropy (CSA) or CSA-DD cross-correlation is negligible, the relaxation parameters for carbons with directly bonded protons can be calculated from the spectral density functions, $J(\omega)$:[44]

$$T_1^{-1} = \frac{1}{4}(\mathrm{DCC})^2[J(\omega_H - \omega_C) + 3J(\omega_C) + 6J(\omega_H + \omega_C)] \quad (1)$$

$$T_2^{-1} = \frac{1}{8}(\mathrm{DCC})^2[4J(0) + J(\omega_H - \omega_C) + 3J(\omega_C) + 6J(\omega_H) + 6J(\omega_H + \omega_C)] \quad (2)$$

$$\eta = \left(\frac{\gamma_H}{\gamma_C}\right)\frac{6J(\omega_H + \omega_C) - J(\omega_H - \omega_C)}{J(\omega_H - \omega_C) + 3J(\omega_C) + 6J(\omega_H + \omega_C)} \quad (3)$$

The dipolar coupling constant, $\mathrm{DCC} = (\mu_0/4\pi)\gamma_C\gamma_H\hbar r_{CH}^{-3}$, where $\mu_0$ is the permittivity of free space; $r_{CH}$ is the proton-carbon internuclear distance; $\gamma_H$ and $\gamma_C$ are the magnetic gyro ratios for proton and carbon, respectively; and $\hbar$ is Planck's constant divided by $2\pi$. A value of 109.8 pm is used for $r_{CH}$, resulting in a DCC of $143.40 \times 10^3$ rad·s$^{-1}$. For carbons with two directly bonded protons the relaxation rates $T_1^{-1}$ and $T_2^{-1}$ can be obtained by multiplying the calculated rates by a factor of 2. It should be noted that eq 2 does not contain any contribution from chemical exchange. This will be commented on below.

(17) Lipari, G.; Szabo, A. *J. Am. Chem. Soc.* **1982**, *104*, 4546−4559; 4559−4570.
(18) Palmer, A. G.; Williams, J.; McDermott, A. *J. Phys. Chem.* **1996**, *100*, 13293−13310.
(19) Luginbül, P.; Pervushin, K. V.; Iwai, H.; Wüthrich, K. *Biochemistry* **1997**, *36*, 7305−7312.
(20) Borer, P. N.; LaPlante, S. R.; Kumar, A.; Zanatta, N.; Martin, A.; Hakkinen, A.; Levy, G. C. *Biochemistry* **1994**, *33*, 2441−2450.
(21) Bouchemal-Chibani, N.; Hervé du Penhoat, C.; Abdelkafi, M.; Ghomi, M.; Turpin, P. Y. *Biopolymers* **1996**, *39*, 549−571.
(22) Bagley, S.; Kovacs, H.; Kowalewski, J.; Widmalm, G. *Magn. Reson. Chem.* **1992**, *30*, 733−739.
(23) Kowalewski, J.; Widmalm, G. *J. Phys. Chem.* **1994**, *98*, 28−34.
(24) Mäler, L.; Lang, J.; Widmalm, G.; Kowalewski, J. *Magn. Reson. Chem.* **1995**, *33*, 541−548.
(25) Mäler, L.; Widmalm, G.; Kowalewski, J. *J. Biomol. NMR* **1996**, *7*, 1−7.
(26) Mäler, L.; Widmalm, G.; Kowalewski, J. *J. Phys. Chem.* **1996**, *100*, 17103−17110.
(27) Kjellberg, A.; Rundlöf, T.; Kowalewski, J.; Widmalm, G. *J. Phys. Chem. B* **1998**, *102*, 1013−1020.
(28) Clore, G. M.; Szabo, A.; Bax, A.; Kay, L. E.; Driscoll, P. C.; Gronenborn, A. M. *J. Am. Chem. Soc.* **1990**, *112*, 4989−4991.
(29) Peng, J. W.; Wagner, G. *J. Magn. Reson.* **1992**, *98*, 308−332.
(30) Peng, J. W.; Wagner, G. *Biochemistry* **1995**, *34*, 16733−16752.
(31) Barbato, G.; Ikura, M.; Kay, L. E.; Pastor, R. W.; Bax, A. *Biochemistry* **1992**, *31*, 5269−5278.
(32) Tjandra, N.; Feller, S. E.; Pastor, R. W.; Bax, A. *J. Am. Chem. Soc.* **1995**, *117*, 12562−12566.
(33) Zhou, L.; Kemple, M. D.; Landy, S. B.; Buckley, P. *J. Magn. Reson. B* **1995**, *109*, 19−30.
(34) Ejchart, A.; Dabrowski, J. *Magn. Reson. Chem.* **1992**, *30*, S115−S124.
(35) Hricovini, M.; Torri, G. *Carbohydr. Res.* **1995**, *268*, 159−175.
(36) Hricovini, M.; Guerrini, M.; Torri, G.; Piani, S.; Ungarelli, F. *Carbohydr. Res.* **1995**, *277*, 11−23.
(37) Poveda, A.; Santamaria, M.; Bernabe, M.; Rivera, A.; Corzo, J.; Jimenez-Barbero, J. *Carbohydr. Res.* **1997**, *304*, 219−228.
(38) Woessner, D. E. *J. Chem. Phys.* **1962**, *37*, 647−654.
(39) Lipari, G.; Szabo, A. *Biochemistry* **1981**, *20*, 6250−6256.
(40) Brüschweiler, R.; Liao, X.; Wright, P. E. *Science* **1995**, *268*, 886−889.
(41) Isbell, H. S.; Pigman, W. *Adv. Carbohydr. Chem. Biochem.* **1969**, *24*, 13−65.
(42) Wertz, P. W.; Garver, J. C.; Anderson, L. *J. Am. Chem. Soc.* **1981**, *103*, 3916−3922.
(43) Lambert, J. B.; Keepers, J. W. *J. Magn. Reson.* **1980**, *38*, 233−244.
(44) Doddrell, D.; Glushko, V.; Allerhand, A. *J. Chem. Phys.* **1972**, *56*, 3683−3689.

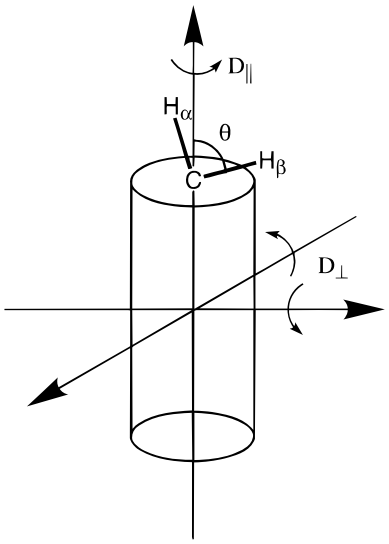


**Figure 2.** Schematic of the axially symmetric model used to fit LNF-1 relaxation data. Rotational diffusion around axes parallel and perpendicular to the unique molecular axis are denoted $D_{||}$ and $D_{\perp}$, respectively. The approximate angles with respect to the unique axis of the $CH_{\alpha}$ and $CH_{\beta}$ vectors of the α and $\beta$ anomeric mixture are depicted.

Different methods have been developed to interpret the relaxation data in terms of motional parameters. As already noted in the Introduction, one of the most widely used is the "model-free" approach developed by Lipari and Szabo.[17] Under the assumption that overall tumbling is isotropic and that its correlation time, $\tau_M$, is much larger than the correlation time for internal reorientation, $\tau_e$, the reduced spectral density function becomes

$$J(\omega) = \frac{2}{5}\left(\frac{S^2\tau_M}{1+\omega^2\tau_M^2} + \frac{(1-S^2)\tau}{1+\omega^2\tau^2}\right) \qquad (4)$$

where $\tau^{-1} = \tau_M{}^{-1} + \tau_e{}^{-1}$. The spatial restriction of the CH vector local motion is described by the generalized order parameter, $S^2$. If the first term of eq 4 is much larger than the second, as in the case of a very rapid internal motion, the second term can be neglected and the equation truncated.

When tumbling is anisotropic, i.e., when the principal rotational diffusion tensors $D_x$, $D_y$, and $D_z$ are nonequal, eq 4 may not be adequate. We follow the approach developed by Tjandra et al.[32] who wrote, for a symmetric top

$$J(\omega) = \frac{2}{5}\left(S^2\sum_{k=1,2,3}A_k\left(\frac{\tau_k}{1+\omega^2\tau_k^2}\right) + \frac{(1-S^2)\tau}{1+\omega^2\tau^2}\right) \qquad (5)$$

where $A_1 = (1.5\cos^2\theta - 0.5)^2$, $A_2 = 3\sin^2\theta\cos^2\theta$, $A_3 = 0.75\sin^4\theta$, $\tau_1 = (6D_{\perp})^{-1}$, $\tau_2 = (5D_{\perp} + D_{||})^{-1}$, and $\tau_3 = (2D_{\perp} + 4D_{||})^{-1}$. As sketched in Figure 2, $\theta$ is the angle between the CH bond vector and the symmetry axis, and $D_{||}$ and $D_{\perp}$ are the elements of the rotational diffusion tensors parallel and perpendicular to this axis, respectively. Tjandra et al. fitted heteronuclear relaxation data to the crystal structure of ubiquitin using this modification, which also included the orientational dependence of each relaxation vector together with internal dynamics. The advantages with this method are that (1) the degree of anisotropy in the rotational diffusion tensor can be investigated by inclusion of the vector orientations in a predefined molecular axes frame and (2) the interpretation of the generalized order parameters and internal correlation times is unchanged.

Though not essential in principle, it is useful to reduce the number of fitting parameters by fixing the angle values when applying the symmetric model free approach. Additionally, different conformations may have to be considered for flexible molecules. The glycosidic linkages for α-L- and $\beta$-D-sugars generally adopt syn conformations, with the torsion angles $\phi$ (H1′−C1′−OX−CX) ∼60° and $\psi$ (C1′−OX−CX−HX) ∼0°,[45] where X is the substituted position. Anti-$\psi$[46] or anti-$\phi$[47] conformations (those where $\psi$ or $\phi$ equals ∼180°) have been shown to be populated but always to a lower extent than the syn conformation. We consider six states of LNF-1, having syn, anti-$\psi$, or anti-$\phi$ conformations at the **D** to **E** linkage and either the α- or $\beta$-configuration at the reducing end. Denoted **a1**, **a2**, **a3** and **b1**, **b2**, **b3**, they were generated with the GEGOP program[48] and subsequently minimized in vacuo using the Quanta-CHARMm (MSI, San Diego, CA) force field parameters. The resulting glycosidic torsion angles for conformation **a1** (assumed to be the most populated state of the α-anomeric configuration) are as follows: $\phi_A = 50°$, $\psi_A = 27°$, $\phi_B = 51°$, $\psi_B = 9°$, $\phi_C = 62°$, $\psi_C = -26°$, $\phi_D = 48°$, and $\psi_D = 6°$. Torsion angles of the **A**−**C** glycosidic linkages adopt similar values for the six conformational states.

The *x*, *y*, and *z* principal components of the moment of inertia tensor were similar for all six structures, with relative values ranging from 1:0.94:0.25 to 1:0.83:0.30. These ratios indicate that the molecule is rodlike, and the use of an axially symmetric molecular model is reasonable. It was then assumed that the principal axis system of the diffusion tensor coincides with the principal frame of the inertia tensor. The eigenvector corresponding to the smallest eigenvalue of the moment of inertia tensor was taken to be the unique molecular diffusion axis, thereby defining $\theta$. The **a2** conformer, with its α-glucose residue flipped around the symmetry axis in the anti-$\psi$ conformation, is expected to show relaxation similar to **a1**, due to similar orientations of the CH vectors.

Langevin dynamics[49] simulations were performed starting from conformation **a1**. Simulations were carried out for 10 ns each, with a time step of 0.002 ps, a collision frequency of 65 $ps^{-1}$, and a dielectric constant of 5.0.

The remainder of this section describes, first in broad terms and then in specific, the hydrodynamic modeling methods used to estimate the rotational and translational diffusion tensors of LNF-1. The methodology, originally developed by Garcia de la Torre and Bloomfield[50] and refined by Wegener,[51] assumes that a molecule can be modeled as a rigid set of N hydrodynamic centers (or beads), interacting via the Oseen tensor. Upon assuming a hydrodynamic radius for each bead and a solution viscosity and temperature, the hydrodynamic properties of the molecule are calculated by inversion of a 3N × 3N matrix. Venable and Pastor applied the bead model to proteins,[52] with

(45) Widmalm, G. Physical methods in carbohydrate research. In *Carbohydrate chemistry*; Boons, G.-J., Ed.; Blackie Academic & Professional: London, 1998; pp 448−502.
(46) Dabrowski, J.; Kozár, T.; Grosskurth, H.; Nifant'ev, N. E. *J. Am. Chem. Soc.* **1995**, *117*, 5534−5539.
(47) Landersjö, C.; Stenutz, R.; Widmalm, G. *J. Am. Chem. Soc.* **1997**, *119*, 8695−8698.
(48) Stuike-Prill, R.; Meyer, B. *Eur. J. Biochem.* **1990**, *194*, 903−919.
(49) Pastor, R. W. In *The molecular Dynamics of Liquid Crystals*; Luckhurst, G. R., Veracini, C. A., Eds.; Kluwer Academic Publishers: Dordrecht, The Netherlands, 1994; pp 85−138.
(50) Garcia de la Torre, J.; Bloomfield, V. A. *Q. Rev. Biophys.* **1981**, *14*, 81−138.
(51) Wegener, W *Biopolymers* **1981**, *20*, 303−326.
(52) Venable, R. M.; Pastor, R. W. *Biopolymers* **1988**, *27*, 1001−1014.

each atom serving as a point of friction. This not only allows a very detailed description of the shape but also requires the addition of "bound water" to reproduce the diffusion constants. Unfortunately, there are no theoretically rigorous methods for adding the water, so distance and energy criteria have been developed to best match independent experimental measurements. As a general observation, the components of the rotational diffusion tensor are much more sensitive to changes in the assumed hydration level than either the translational diffusion constant or the rotational anisotropy. Because this represents our first application to carbohydrates, calculations were carried out on sucrose at different hydration levels for calibration purposes.

Atomic coordinates for the six LNF-1 models and the neutron diffraction crystal structure of sucrose[53] were solvated using the program CHARMM[54] with the TIP3P water model, in either a 30 Å (LNF-1) or a 20 Å (sucrose) cubic box. Each of the seven structures was solvated three times, with the water box rotated by 90° increments around the Cartesian *Y* axis (0, 90, and 180), to produce variations in the placement of solvent molecules around the solute. Each box was energy minimized using periodic images and Ewald summation, in two discrete stages: (1) 50 steps of steepest descent minimization with all solute atoms fixed and (2) 500 steps of Adopted Basis Newton Raphson minimization, with a gradient tolerance of $10^{-3}$ kcal·mol$^{-1}$· Å$^{-1}$ and no constraints. After the minimization, solvation shells were defined by two different criteria: (1) all water oxygen atoms within 3.7 Å of any solute heavy atom, as previously used for proteins[55] and (2) a series of water−solute interaction energy cutoffs based on integer multiples of $-kT$, ranging from 1 to 4. The coordinates for solvent shell oxygen atoms and the solute heavy atoms were saved as subsets for each of the 21 structures, with the hydrodynamic radii of solute heavy atoms and water oxygens set to 1.0 and 1.6 Å, respectively. We emphasize that the placement of water is ad hoc, but that estimates of the rotational anisotropy and translational diffusion constant are insensitive to small changes in the methodology (e.g., energy minimization as opposed to molecular dynamics simulation).

The heavy atom coordinates and radii for the 105 subsets (one distance and four energy criteria for each of the 21 solvations) were used as input to the hydrodynamics program, currently denoted HI5 (for Hydrodynamic Interaction, version 5). The viscosity of the 0.1 M deuterated water solution of LNF-1 was estimated to be 1.4 ± 0.1, based on the model of Chirife and Buera[56] and adjusting for the higher relative viscosity of $D_2O$ (1.2).[57] In the Chirife-Buera model, developed predominantly with mono- and disaccharide data, the relative viscosity is given by the following: $\mu = a \cdot \exp(XE)$, where $a$ is a constant close to unity, $X$ is the mole fraction of oligosaccharide, and $E$ is a molecular constant obtained by extrapolation to a value of 154.07, based on the molecular weight of LNF-1 (853.3 amu). Calculated hydrodynamic quantities scale linearly with the viscosity and should be understood to reflect the 5−10% uncertainty in this quantity. The temperature was set to be that of the NMR probe, 303 K. The sucrose calculations assumed infinite dilution at 293 K and a viscosity of 1.0 cp.

## Experimental Section

Natural abundance lacto-*N*-fucopentaose-1 (60 mg) was treated with CHELEX 100 in order to remove paramagnetic ions. The freeze-dried oligosaccharide was dissolved in 0.7 mL of $D_2O$ to a 0.1 M solution and transferred to a 5 mm NMR tube. Oxygen was removed by three freeze−pump−thaw cycles, and finally the NMR tube was sealed under vacuum. Assignments of the carbon-13 chemical shifts have been reported earlier.[58] Measurements were performed at 303 ± 2 K and four magnetic field strengths (7.04, 9.39, 11.75, 14.09 T) using Varian Unity or Inova spectrometers equipped with broad band or carbon-13 probes. Deuterium lock was used for frequency/field stabilization, and the proton decoupler was attenuated in order to avoid sample heating. The spectral width was ~120 ppm and 16k complex data points were sampled. The FIDs were multiplied with a 5 Hz exponential line broadening factor prior to Fourier transformation. At 11.75 and 14.09 T 25 signals were well resolved and used for measurements. At the two lower fields 21 signals were used. Relaxation data are averages of 3−8 independent measurements at each magnetic field. Temperature calibrations were carried out using the proton shift thermometer[59] and/or an electronic thermometer calibrated in ice and boiling water.

Carbon-13 $T_1$ measurements were performed at all magnetic field strengths by fast inversion−recovery experiments,[60] using three-parameter nonlinear fits of line intensities. Ten different relaxation delay times (10 ms to ~5 $T_1$) were used, and the prescan delay was ~3$T_1$. The average standard deviation of $T_1$ was 3−5% between experiments for any peak.

Carbon-13 $T_2$ were measured at 9.4 and 14.1 T using a modification of the CPMG pulse sequence, with proton $\pi$ pulses of 26 and 46 $\mu$s, respectively, placed at even echos in order to minimize cross-correlation effects.[61,62] The carbon $\pi$ pulses were 14 and 11 $\mu$s, respectively, at the two fields. Twelve different relaxation delays (2 ms to ~1.5$T_2$) were used, the CPMG delay was set to 0.25 ms, and the prescan delay was > 10$T_1$. The average standard deviation of $T_2$ was 7−14%.

Heteronuclear $^1$H−$^{13}$C NOE was measured with the dynamic NOE technique.[63] The experiments were performed with one short (1 ms) and one long (~5$T_1$) irradiation period and a prescan delay of > 10$T_1$. The NOEs ($1 + \eta$) were calculated by taking the ratio of the intensity at the long irradiation period to that of the short one. The average standard deviation of $1 + \eta$ was 1−3%.

The magnetic field dependent $T_1^{-1}$, $T_2^{-1}$, and $1 + \eta$ values of resolved peaks were least-squares fitted at all magnetic fields simultaneously using the program GENLSS[64] running on an SGI workstation, resulting in model-free parameters $S^2$, $\tau_M$, and $\tau_e$ in the case of isotropic overall reorientation and $S^2$, $\tau_{M,eff}$, $D_{||}/D_{\perp}$, and $\tau_e$ for anisotropic reorientation. Sums of squares of relative (rather than absolute) errors were minimized, allowing the measured parameters ($T_1^{-1}$, $T_2^{-1}$, and $1 + \eta$) to be treated in a balanced way.

Translational diffusion measurements were performed at 303 K on a Bruker AMX 300 MHz NMR spectrometer using the three-pulse stimulated-echo pulsed-gradient spin−echo technique,[65,66] with 1 ms gradient pulses and spacings between the 90° pulses of 10 and 90 ms, respectively.

## Results and Discussion

Carbon-13 relaxation measurements were performed for 21 or 25 well resolved peaks at the lower or higher magnetic field

(53) Brown, G. M.; Levy, H. A. *Acta Crystallogr.* **1973**, *B29*, 790−797.
(54) Brooks, B. R.; Bruccoleri, R. E.; Olafson, B. D.; States, D. J.; Swaminathan, S.; Karplus, M. *J. Comput. Chem.* **1983,** *4*, 187−217.
(55) Copié, V.; Tomita, Y.; Akiyama, S. K.; Aota, S.-i.; Yamada, K. M.; Venable, R. M.; Pastor, R. W.; Krueger, S.; Torchia, D. A. *J. Mol. Biol.* **1998**, *277*, 663−682.
(56) Chirife, J.; Buera, M. F. *J. Food Eng.* **1997**, *53*, 221−226.
(57) Mills, R.; Harris, K. R. *Chem. Soc. Rev.* **1976**, *5*, 215−231.
(58) Hermansson, K.; Jansson, P.-E.; Kenne, L.; Widmalm, G.; Lindh, F. *Carbohydr. Res.* **1992**, *235*, 69−81.
(59) Ammann, C.; Meier, P.; Merbach, A. E. *J. Magn. Reson.* **1982**, *46*, 319−321.
(60) Canet, D.; Levy, G. C.; Peat, I. R. *J. Magn. Reson.* **1975**, *18*, 199−204.
(61) Kay, L. E.; Nicholson, L. K.; Delaglio, F.; Bax, A.; Torchia, D. A. *J. Magn. Reson.* **1992**, *97*, 359−375.
(62) Palmer, A. G.; Skelton, N. J.; Chazin, W. J.; Wright, P. E.; Rance, M. *Molec. Phys.* **1992**, *75*, 699−711.
(63) Kowalewski, J.; Ericsson, A.; Vestin, R. *J. Magn. Reson.* **1978**, *31*, 165−169.
(64) DeTar, D. F. GENLSS. In *Computer programs for chemistry*; Academic Press: New York, 1972; Vol. 4; pp 71−124.
(65) Tanner, J. E. *J. Chem. Phys.* **1970**, *52*, 2523−2526.
(66) Stilbs, P. *Progr. NMR Spectr.* **1987**, *19*, 1−45.

**Table 1.** Carbon-13 Relaxation Data for LNF-1 at 30 °C and Four Magnetic Fields Strengths

| | 7.04 T | | 9.39 T | | | 11.75 T | | 14.09 T | | |
|---|---|---|---|---|---|---|---|---|---|---|
| atom[a] | $T_1$[b] | $1+\eta$ | $T_1$ | $T_2$[b] | $1+\eta$ | $T_1$ | $1+\eta$ | $T_1$ | $T_2$ | $1+\eta$ |
| **A** 1 | 187 | 1.98 | 227 | 196 | 1.74 | 270 | 1.55 | 305 | 253 | 1.46 |
| **A** 2 | 202 | 2.02 | 239 | 202 | 1.85 | 278 | 1.69 | 312 | 265 | 1.60 |
| **A** 3 | 201 | 2.02 | 242 | 220 | 1.85 | 282 | 1.67 | 316 | 255 | 1.59 |
| **A** 4 | 200 | 1.89 | 239 | 202 | 1.78 | 277 | 1.54 | 315 | 250 | 1.49 |
| **A** 5 | 200 | 1.95 | 233 | 194 | 1.94 | 268 | 1.68 | 302 | 263 | 1.59 |
| **B** 1 | 206 | 2.11 | 242 | 203 | 1.89 | 284 | 1.67 | 319 | 258 | 1.60 |
| **B** 2 | 204 | 2.09 | 239 | 213 | 1.92 | 273 | 1.71 | 310 | 274 | 1.64 |
| **B** 3 | 213 | 2.06 | 250 | 233 | 1.88 | 289 | 1.73 | 326 | 261 | 1.64 |
| **B** 4 | 210 | 2.15 | 241 | 211 | 1.95 | 279 | 1.76 | 313 | 251 | 1.65 |
| **B** 5 | *c* | *c* | *c* | *c* | *c* | 293 | 1.71 | 328 | 270 | 1.64 |
| **B** 6 | *c* | *c* | *c* | *c* | *c* | 222 | 2.13 | 242 | 217 | 2.08 |
| **C** 1 | 204 | 2.16 | 246 | 197 | 1.96 | 279 | 1.68 | 318 | 264 | 1.63 |
| **C** 2 | 195 | 2.13 | 229 | 179 | 1.97 | 264 | 1.74 | 300 | 214 | 1.65 |
| **C** 3 | 206 | 2.18 | 238 | 219 | 1.96 | 273 | 1.74 | 306 | 228 | 1.65 |
| **C** 5 | *c* | *c* | *c* | *c* | *c* | 282 | 1.64 | 316 | 233 | 1.65 |
| **C** 6 | *c* | *c* | *c* | *c* | *c* | 218 | 2.06 | 242 | 207 | 2.03 |
| **D** 1 | 242 | 2.16 | 284 | 245 | 2.02 | 321 | 1.74 | 372 | 287 | 1.74 |
| **D** 3 | 229 | 2.09 | 271 | 212 | 1.97 | 302 | 1.79 | 342 | 310 | 1.73 |
| **D** 6 | 121 | 2.13 | 140 | 120 | 1.91 | 165 | 1.74 | 181 | 160 | 1.65 |
| $\mathbf{E}_\alpha$ 1 | 207 | 2.16 | 248 | 212 | 1.88 | 295 | 1.62 | 325 | 252 | 1.49 |
| $\mathbf{E}_\alpha$ 2 | 303 | 2.05 | 353 | 316 | 2.05 | 400 | 1.94 | 445 | 350 | 1.89 |
| $\mathbf{E}_\alpha$ 3 | 298 | 2.00 | 349 | 321 | 2.11 | 404 | 1.93 | 439 | 325 | 1.87 |
| $\mathbf{E}_\beta$ 1 | 318 | 2.21 | 378 | 314 | 2.08 | 419 | 1.92 | 473 | 311 | 1.84 |
| $\mathbf{E}_\beta$ 2 | 304 | 2.21 | 356 | 277 | 2.12 | 399 | 1.92 | 451 | 331 | 1.86 |
| $\mathbf{E}_\beta$ 3 | 289 | 2.09 | 358 | 298 | 2.06 | 401 | 1.95 | 452 | 373 | 1.88 |

[a] Sugar residue in bold followed by carbon atom number. [b] Relaxation time (ms). [c] Not measured.

strengths, respectively, fairly equally distributed over the different sugar residues. The molecule resides outside the extreme narrowing regime at all studied magnetic fields, in the region where the $^1H-^{13}C$ NOE, $T_1$, and $T_2$ are all field dependent, and $T_1 \neq T_2$.

Relaxation data, listed in Table 1, clearly show motional differences between CH vectors in different sugar residues and sometimes also between neighboring vectors within a sugar residue. Similar $T_1$ differences to those for residue **E** between the $\alpha$ and $\beta$ anomeric carbons at the reducing end have been observed for $\alpha$-(1→4)-linked glucose oligosaccharides.[67] For the exocyclic hydroxymethyl carbons at the **B**−**D** residues differences are clearly seen, with $T_1$, $T_2$, and NOE values of **D** C6 significantly lower, and also similar to the methine carbons in **D**, than to the hydroxymethyl carbons of **B** and **C**.

In our previous studies of motional properties of oligosaccharides we treated the ring-skeletons of the sugar residues as "dynamically equivalent",[23] with $T_1$, $T_2$, and NOE data averaged for each sugar ring at every magnetic field, since the methine carbon relaxation parameters within each sugar residue were quite similar. The concept of "dynamic equivalence" has been shown to be useful in other applications.[68] However, the present relaxation data raises the question whether such a treatment is justified for LNF-1. The observed differences in relaxation parameters could be arising from motional anisotropy, differences in internal motions or a combination of both.

In principle, chemical (conformational) exchange effects might cause deviations from the dynamic equivalence, at least for the transverse relaxation. This possibility can safely be excluded in the present case. We follow the reasoning of Phan et al.[69] who showed that exchange effects can be expected to

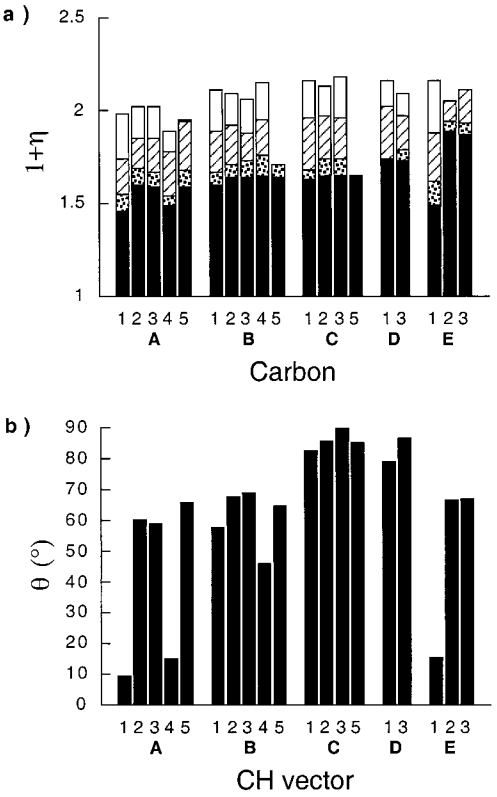


**Figure 3.** (a) Experimental NOE data at 7.0 T (open), 9.4 T (dashed lined), 11.7 T (dotted), and 14.1 T (black) and (b) CH vector orientations ($\theta$) for structure **a1**. Sugar residues are denoted **A**−**E**, and CH vectors are numbered after their corresponding carbon atoms.

increase with the square of the magnetic field. More specifically, in the absence of CSA relaxation (a reasonable assumption for the carbons investigated in the sugar residues), the quantity $\Delta = T_2^{-1} - T_1^{-1}/2$ should increase with the square of the field. From the data in Table 1, $\Delta$ can be obtained at two fields (9.4 and 14.1 T). For 18 out of 21 carbons for which the relaxation data at both fields are available, $\Delta$ actually decreases or remains unchanged between 9.4 and 14.1 T. For the remaining three carbons (C3 in **C**, C3 in $\mathbf{E}_\alpha$, and C1 in $\mathbf{E}_\beta$) $\Delta$ increases but only slightly. Thus, we conclude that the chemical exchange effects are not significant.

Figure 3 shows NOE data and CH vector orientations in the **a1** model. The NOE differences between axial and equatorial CH vectors in the **A** residue, also showing different $\theta$, provide a natural entry point for determination of rotational diffusion anisotropy. Three groups of orientations are observed for the individual methine vectors: (1) $\theta \sim 10°$ for C1 and C4 in **A** and C1 in $\mathbf{E}_\alpha$; (2) $\theta \sim 45°$ for C4 of **B**; and (3) $\theta = 60°-90°$ for all others.

Using the specific CH vector orientations in residue **A** of structure **a1**, model-free motional parameters were fitted to the experimental relaxation data using eq 5 (axially symmetric) and eq 4 (isotropic). The results are listed in rows 1 and 2 of Table 2. The axially symmetric model yields a slightly better fit ($\Delta y = 3.3\%$ vs 3.9% for the isotropic model) and an anisotropy of 1.35. Values of $\tau_e$ and $S^2$ are comparable. Residues **B**, **C**, **D**, $\mathbf{E}_\alpha$, and $\mathbf{E}_\beta$ were then fitted with $D_\parallel/D_\perp$ fixed at 1.35 and also isotropically. As for **A**, the results were comparable for isotropic and anisotropic fits, including a negative (and therefore unphysical) value for the fast correlation time for residue $\mathbf{E}_\alpha$ and

(67) Kadkhodaei, M.; Wu, H.; Brant, D. A. *Biopolymers* **1991**, *31*, 1581−1592.

(68) Lippens, G.; Wieruszeski, Horvath, D.; Talaga, P.; Bohin, J.-P. *J. Am. Chem. Soc.* **1998**, *120*, 170−177.

(69) Phan, I. Q. H.; Boyd, J.; Campbell, I. D. *J. Biomol. NMR* **1996**, *8*, 369−378.

**Table 2.** Results from Least-Squares Fits of the Model-Free Parameters to the $^{13}C$ Relaxation Data Measured for Methine (CH) and Methylene ($CH_2$) Carbons of LNF-1, Using Isotropic (iso) and Axially Symmetric[a] (ax) Models

| residue | type of carbon | type of fit | $\tau_{M,eff}$[b] (ns) | $D_{\|\|}/D_\perp$ | $S^2$ | $\tau_e$ (ps) | $\Delta y$[c] (%) |
|---|---|---|---|---|---|---|---|
| **A** | CH | ax | $0.61 \pm 0.02$ | $1.35 \pm 0.09$ | $0.75 \pm 0.02$ | $27 \pm 12$ | 3.3 |
| | CH | iso | $0.63 \pm 0.03$ | 1 | $0.74 \pm 0.02$ | $29 \pm 14$ | 3.9 |
| **B** | CH | ax | $0.59 \pm 0.02$ | 1.35[d] | $0.72 \pm 0.02$ | $47 \pm 12$ | 3.0 |
| | CH | iso | $0.59 \pm 0.02$ | 1 | $0.71 \pm 0.02$ | $48 \pm 11$ | 2.9 |
| | $CH_2$ | iso | 0.61 | 1 | $0.30 \pm 0.01$ | $70 \pm 4$ | 2.1 |
| **C** | CH | ax | $0.64 \pm 0.05$ | 1.35[d] | $0.72 \pm 0.05$ | $77 \pm 25$ | 5.1 |
| | CH | iso | $0.62 \pm 0.05$ | 1 | $0.71 \pm 0.05$ | $80 \pm 24$ | 5.1 |
| | $CH_2$ | iso | 0.61 | 1 | $0.33 \pm 0.01$ | $65 \pm 2$ | 0.9 |
| **D** | CH | ax | $0.62 \pm 0.06$ | 1.35[d] | $0.60 \pm 0.05$ | $57 \pm 18$ | 4.5 |
| | CH | iso | $0.60 \pm 0.05$ | 1 | $0.60 \pm 0.05$ | $58 \pm 18$ | 4.4 |
| | $CH_2$ | iso | 0.61 | 1 | $0.59 \pm 0.01$ | $41 \pm 8$ | 3.0 |
| $\mathbf{E}_\alpha$ | CH | ax | $0.50 \pm 0.04$ | 1.35[d] | $0.80 \pm 0.05$ | $(-23 \pm 42)$[f] | 3.1 |
| (C1) | CH | ax | 0.61[e] | 1.35 | $0.68 \pm 0.02$ | $40 \pm 14$ | 4.2 |
| | CH | iso | $0.55 \pm 0.04$ | 1 | $0.80 \pm 0.05$ | $(-23 \pm 42)$[f] | 3.1 |
| $\mathbf{E}_\alpha$ | CH | ax | $0.81 \pm 0.07$ | 1.35[d] | $0.35 \pm 0.02$ | $69 \pm 5$ | 3.8 |
| (C2−3) | CH | ax | 0.61[e] | 1.35 | $0.43 \pm 0.01$ | $54 \pm 5$ | 4.0 |
| | CH | iso | $0.79 \pm 0.07$ | 1 | $0.35 \pm 0.02$ | $69 \pm 5$ | 3.7 |
| $\mathbf{E}_\beta$ | CH | ax | $0.78 \pm 0.07$ | 1.35[d] | $0.35 \pm 0.02$ | $67 \pm 6$ | 4.8 |
| (C1−3) | CH | ax | 0.61[e] | 1.35 | $0.42 \pm 0.01$ | $52 \pm 4$ | 4.1 |
| | CH | iso | $0.77 \pm 0.07$ | 1 | $0.35 \pm 0.02$ | $68 \pm 6$ | 4.8 |

[a] Data are fitted using eq 5 and orientations of methine CH vectors in the **a1**/**b1** model. [b] $\tau_{M,eff}$ is calculated from $(2D_{\|} + 4D_\perp)^{-1}$. [c] Standard deviation of dependent parameter. [d] $D_{\|}/D_\perp$ is fixed to the value obtained for the **A** residue (see text). [e] $\tau_{M,eff}$ and $D_{\|}/D_\perp$ are fixed to the values obtained for the **A** residue. [f] Unphysical.

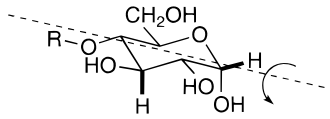


**Figure 4.** The **E** residue in its α-configuration, showing the axis around which internal dynamics occur (dashed line). CH vectors axial ($S^2 = 0.43$) and equatorial ($S^2 = 0.68$) with respect to the plane of the sugar ring and to the axis are shown in bold.

significantly different values for the slow correlation time for this residue (Table 2).

To further explore the anomalous behavior of residue **E**, the data were fitted without constraints on the anisotropy. This yielded, $D_{\|}/D_\perp = 4.1 \pm 0.8$, similar to the anisotropy in the moment of inertia tensor but unrealistic compared to hydrodynamics estimates (discussed below) and a substantial error ($\Delta y = 10\%$). Additionally, when fits were carried out for the other residues using the preceding anisotropy, substantially larger errors were obtained compared to those observed in the isotropic fits.

Given that attempts to explain the relaxation behavior of the ring carbons in residue **E** in terms of molecular anisotropy were unsuccessful, it is reasonable to consider internal dynamics in more detail. An internal rotation of the $\psi$ torsion angle of the glycosidic linkage between residues **D** and **E** should result in a low order parameter for a CH vector of perpendicular orientation to that motion, i.e., the axial CH vectors in $\mathbf{E}_\alpha$, whereas the relaxation of the equatorial α-anomeric CH vector, oriented parallel to the motional axis, should be insensitive to that motion (Figure 4). The opposite relationship should hold for the **a3** anti-$\phi$ conformer. This notion can be used to explain the particular values of the fitted parameters for C1 in $\mathbf{E}_\alpha$, cf. Table 2. The three-parameter fits result in a high value of the order parameter (in fact, so high that the local correlation time is no longer possible to estimate, leading to the unphysical negative values in Table 2). In contrast, the axial CH vectors in $\mathbf{E}_\alpha$ (as well as in $\mathbf{E}_\beta$, cf. **b1** and **b2**) behave in the way expected for a "floppy" terminal ring, i.e., fitting yields a low order parameter. The overall fitted rotational correlation times for these CH vectors are longer than for the other rings, though the origin of this deviation from the model is not quite clear. It is also possible to investigate the anisotropy of the local dynamics, i.e., the sensitivity of individual CH vectors to internal motions, in the residues **A**−**D**. For the **A** residue, the CH vectors with equatorial and axial orientation with respect to the sugar ring showed differences in the NOE data. To interpret this observation in terms of internal dynamics, separate isotropic fits were carried out for each of the five carbons, using the truncated version of eq 4 (data not shown). The motional behavior of C1/C4 was rather similar to that of C2/C3/C5, with $S^2 \approx 0.8$, and only small differences for the overall correlation time reflecting anisotropy of the overall reorientation. For residues **B**−**D**, the fits of this type showed no remarkable differences between individual methine carbons. Taken together, these observations clearly demonstrate that the internal dynamics of residue $\mathbf{E}_\alpha$ differs from that of **A**−**D**.

Two-parameter least-squares fits of relaxation data for the exocyclic methylene carbons of residues **B**−**D** were performed, using eq 4, making the assumptions that each of the two CH vectors contribute equally to the measured relaxation times and that the correlation time for the overall motion could be fixed at 0.61 ns. Different results were obtained for the exocyclic carbons of the **B** and **C** residues compared to residue **D**. Residues **B** and **C** showed low order parameters, $S^2 \approx 0.3$ and $\tau_e \approx 70$ ps for the exocyclic carbons, while the motions of C6 in the **D** residue was found to be substantially more restricted, with $S^2 \approx 0.6$ and $\tau_e \approx 40$ ps, showing similar motional freedom as the methine carbons of this residue. The errors in the fits were found to be rather small, $\Delta y < 3\%$. Differences in the motional parameters between exocyclic carbons were previously reported, e.g. for the trisaccharide melezitose.[24] The exocyclic carbon C1 in the fructofuranosyl residue of this trisaccharide was found to have a higher order parameter ($S^2 \approx 0.75$) than the exocyclic carbon C6 in the same residue ($S^2 \approx 0.6$). Local correlation times of a few tens of picoseconds were obtained for the exocyclic carbons, similar to the local correlation time found for C6 in **D** of LNF-1. The hydroxymethyl groups of the **B** and **C** residues showed significantly lower order parameters and longer local correlation times compared to both the **D** residue in LNF-1 and to the corresponding values observed for melezitose. The low order parameters of the hydroxymethyl

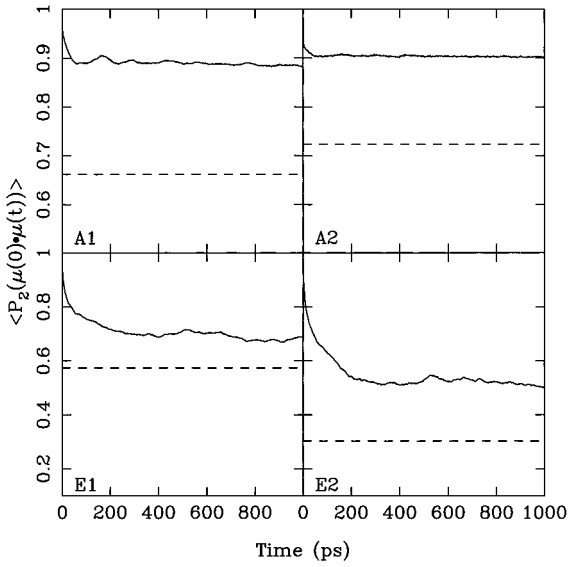


**Figure 5.** Reorientational correlation functions (solid lines) for the CH vectors of carbons 1 and 2 of residues **A** and **E** from Langevin dynamics simulations, with the other residues fixed. Dashed lines show the generalized order parameters from simulations where only residue **C** was fixed, and torsion angle values not associated with conformation **a1** were excluded. Note that the ordinate range for residue **A** is 0.5−1.0.

groups of the **B** and **C** residues reveal quite extensive motions, suggesting a large degree of conformational flexibility for these exocyclic groups.

To further investigate the motions of LNF-1 two sets of Langevin dynamics simulations were performed starting from the **a1** conformation. In set I, residues **A**−**D** were fixed in simulation of **E**, and residues **B**−**E** were fixed in simulation of **A**. This procedure yields an upper limit for the generalized order parameters of **E** and **A**, respectively; i.e., flexibility of residues **B** and **D** should reduce the order parameters of the neighboring residues. In set II, only residue **C** was fixed, providing an estimate of the maximum effect of flexibility within a single conformation. Given that waters were not included and that the potential is relatively undeveloped, these simulations were carried out solely to determine if the order parameters of residue **E** can be plausibly explained by fluctuations in a single conformation, or whether transitions between conformations are necessary.

The solid lines in Figure 5 show the reorientational correlation functions for the CH vectors of carbons 1 and 2 of residues **A** and **E** for set I. The plateau values (equal to $S^2$) for both carbons of residue **A** are approximately 0.9, whereas those of residue **E** are 0.71 and 0.54 for carbons 1 and 2, respectively. These values qualitatively agree with those in Table 2 for the axially symmetric fits with fixed $\tau_{M,eff} = 0.61$ ns, especially with regard to the differences of C1 and C2 in **E**. The time scale of the relaxation of residue **E** is substantially longer than for **A**, which also agrees with the fitted results.

The generalized order parameters for set II, plotted as dashed lines in Figure 5, were obtained by including torsion angles only in conformation **a1**. For residue **A** they are 0.66 and 0.72 for C1 and C2, respectively; for residue **E** they are 0.57 and 0.30 for the corresponding carbons. When other conformations (the result of isomerizations during the simulation) were added, the order parameters of residue **E** were close to zero. This suggests that isomerizations may be taking place on a time scale close to or longer than molecular tumbling and therefore difficult to obtain from model free fitting of the relaxation data.

**Table 3.** Comparison of Calculated and Measured Diffusion Data for LNF-1 and Sucrose

| shell cutoff | $N_{water}$[f] | $D_{\|\|}/D_\perp$ | $(I_\perp/I_{\|\|})^{0.7}$ | $\tau_M$ (ns) | $D_t \times 10^{-6}$ ($cm^2\ s^{-1}$) |
|---|---|---|---|---|---|
| LNF-1 at 30 °C (**a1** Conformer) | | | | | |
| $d = 3.7$[a] | 45.0 | 1.63 | 1.81 | 0.9 | 2.0 |
| -1$kT$[b] | 61.7 | 1.62 | 1.73 | 1.2 | 1.7 |
| -2$kT$ | 33.3 | 1.73 | 1.93 | 0.8 | 2.0 |
| -3$kT$ | 21.0 | 1.84 | 2.06 | 0.7 | 2.1 |
| -4$kT$ | 13.0 | 2.17 | 2.27 | 0.5 | 2.3 |
| expt | | | | *0.6*[c] | *1.8*[c] |
| Sucrose at 20 °C | | | | | |
| $d = 3.7$ | 22.4 | 1.26 | 1.31 | 0.21 | 3.8 |
| -1$kT$ | 35.7 | 1.24 | 1.25 | 0.41 | 3.0 |
| -2$kT$ | 18.0 | 1.25 | 1.28 | 0.19 | 3.9 |
| -3$kT$ | 12.0 | 1.38 | 1.35 | 0.14 | 4.3 |
| -4$kT$ | 10.0 | 1.38 | 1.35 | 0.12 | 4.5 |
| -5$kT$ | 6.0 | 1.54 | 1.42 | 0.09 | 5.0 |
| expt | | | | *0.12*[d] | *4.6*[e] |

[a] Distance in Å. [b] Interaction energy. [c] This work. [d] Reference 71. [e] Reference 72. [f] $N_{water}$, the number of waters assumed to be hydrodynamically bound to the solute, appears as a fraction because the results are averaged over three different solvations.

The translational diffusion coefficient of LNF-1 was measured at 303 K by the stimulated-echo technique.[65,66] A value of 1.8 $\times$ $10^{-6}$ $cm^2\ s^{-1}$ was obtained. This can be compared to the previously determined diffusion coefficient of 2.7 $\times$ $10^{-6}$ $cm^2\ s^{-1}$ for a trisaccharide in $D_2O$ at 293 K.[70]

The results of the hydrodynamics calculations of translational and rotational diffusion data for LNF-1 and sucrose[71,72] are summarized in Table 3. We first consider sucrose. The estimates of $\tau_M$ and $D_t$ clearly indicate that the solvation protocol previously applied to large proteins (a distance cutoff of 3.7 Å) overestimates the number of water molecules in the solvation shell for sucrose. An interaction energy based cutoff provides a convenient means to generate a series of solvation shells, but the energy values are somewhat approximate and should not be overinterpreted. Table 3 shows that the distance cutoff is similar to a solvation shell with a cutoff of $-2kT$, whereas a cutoff of $-4kT$ provides better agreement with experiment. These results suggest that about one water molecule per free hydroxyl (or polar) group is an appropriate model for solvation of small oligosaccharides. Similar results were obtained for ethylene glycol[73] and glycine and a dipeptide.[52] The level of sucrose hydration also agrees with an estimate based on intrinsic viscosity originally published by Einstein in 1906.[74]

Assuming at least two bound water molecules for the *N*-acetyl group and one per hydroxyl group leads to an estimate of 17 bound waters for LNF-1 (Figure 6 depicts a typical coordinate set). From Table 3, this level of hydration falls between the $-3kT$ and $-4kT$ cutoffs and is much lower than that obtained using the distance cutoff. The isotropic relaxation time computed for these two energy cutoffs bracket the NMR value of 0.6 ns, but the computed translational diffusion constant is approximately 20% higher than experiment. A larger number of bound waters or a higher effective viscosity lowers $D_t$ but raises $\tau_M$. Fortunately, the rotational anisotropy is relatively insensitive

(70) Widmalm, G.; Venable, R. M. *Biopolymers* **1994**, *34*, 1079−1088.
(71) Hervé du Penhoat, C.; Imberty, A.; Roques, N.; Michon, V.; Mentech, J.; Descotes, G.; Perez, S. *J. Am. Chem. Soc.* **1991**, *113*, 3720−3727.
(72) van Holde, K. E. *Physical Biochemistry*, 2nd ed.; Prentice-Hall: Englewood Cliffs, NJ, 1985; p 103.
(73) Widmalm, G.; Pastor, R. W. *J. Chem. Soc., Faraday Trans.* **1992**, *88*, 1747−1754.
(74) Einstein, A. *Investigations on the Theory of Brownian Movement*; Dover, NY, 1956; pp 54−56.

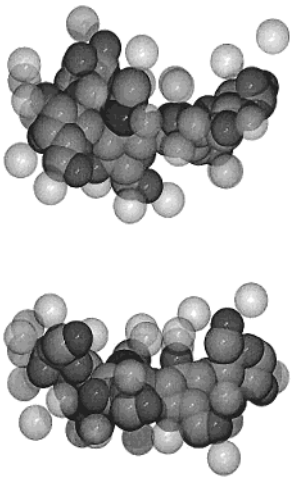

**Figure 6.** A heavy atom space filling model of LNF-1 in the **a1** conformation showing two orthogonal views with bound waters (cutoff $= -3kT$) represented as transparent. The reducing residue **E** is to the right.

to these details and can be estimated to be $1.8 \pm 0.2$. Least-squares fits of the model-free parameters to the relaxation data for all sugar residues were repeated with this anisotropy as a fixed value (not shown). Motional parameters and errors similar to those in the corresponding isotropic fits were observed. We note, however, that of the relaxation parameters the NOE data were of the highest quality and also clearly orientation dependent (Figure 3). Fitting the NOE data of residue **A**, using the motional parameters in row one of Table 2, resulted in an increase of the anisotropy to 1.5. In the study of fibronectin cell attachment modules,[55] the rotational anisotropy determined by $^{15}$N $T_1$ and $T_2$ relaxation was also somewhat lower than calculated by hydrodynamic modeling. It is probable that flexibility of both of these systems can account for the decrease in anisotropy estimated from rigid body modeling.

Last, the third and fourth columns of Table 3 confirm the approximate relation derived for symmetric tops:[55]

$$\frac{D_{||}}{D_{\perp}} \approx \left(\frac{I_{\perp}}{I_{||}}\right)^{0.7} \tag{6}$$

This relationship holds well for both sucrose and LNF-1, when hydrodynamically bound waters are included. It underscores that, in general, assuming that the rotational anisotropy is directly proportional to $I_{\perp}/I_{||}$ leads to large overestimates of the former.

## Conclusions

The motional properties of the pentasaccharide lacto-*N*-fucopentaose-1 have been investigated by carbon-13 nuclear spin relaxation at different magnetic fields. The flexibility of the sugar residues of the α anomeric state could be described in terms of the generalized order parameter, $S^2$, with values of 0.6−0.75, except for carbons 2 and 3 of the reducing sugar residue **E** where $S^2 = 0.43$. The low order parameters for these latter two carbons arise from their orientation with respect to the axis of libration (Figure 4) and the substantial flexibility of this residue (Figure 5), rather than isomerization between different conformations. The order parameters for residue **E** as the $\beta$ anomer are all low by an analogous geometrical interpretation.

Even though the overall rotational anisotropy ($D_{||}/D_{\perp}$) was determined to be 1.35 (all relaxation data) or 1.5 (NOE only), the order parameters and fast and slow correlation times were similar to those obtained using an isotropic model. This underscores some potential difficulties in using the anisotropic model free formalism associated with the relative insensitivity of the parameters associated with fast motions to parameters of the slow motions. Nevertheless, it is reasonable to eliminate the effects of anisotropy in fitting before making conclusions about flexibility when studying a new system.

Comparison of the experimentally determined translational diffusion coefficient and that calculated by hydrodynamic modeling led to an estimate of approximately one water molecule per hydroxyl group of the pentasaccharide. Based on this hydration level, hydrodynamic calculations yielded a rotational anisotropy of 1.8, which is somewhat higher than the range obtained from fitting to experiment. The results of bead model hydrodynamic calculations are best used to provide plausible ranges of values for the relaxation time or the anisotropy of a specific conformation. If experimental values differ significantly, the presence of higher than expected internal motions or completely different conformations should be considered. In this case, the time scale and level of libration and its possible coupling with molecular tumbling require further study.

**Acknowledgment.** The Swedish Natural Science Research Council is acknowledged for financial support. We thank professor Peter Stilbs at Kungliga Tekniska Högskolan, Stockholm, Sweden for help with the NMR diffusion measurements. The Swedish NMR center is thanked for providing access to the U300, U500, and U600 NMR spectrometers.

JA992675B